Available online at www.sciencedirect.com
ScienceDirect
Trans. Nonferrous Met. Soc. China 20(2010) 1217−1221
Transactions of Nonferrous Metals Society of China
www.tnmsc.cn

Fracture behavior of high strength Mg-Gd-Y-Zr magnesium alloy

GAO Lei(高 磊)[1,2], CHEN Rong-shi(陈荣石)[1], HAN En-hou(韩恩厚)[1]

1. State Key Laboratory for Corrosion and Protection, Institute of Metal Research, Chinese Academy of Sciences, Shenyang 110016, China;
2. Graduate School of Chinese Academy of Sciences, Beijing 100039, China

Received 23 September 2009; accepted 30 January 2010

Abstract: The fracture behavior of a permanent mould casting Mg-8.57Gd-3.72Y-0.54Zr (mass fraction, %) (GW94) alloy was investigated under different thermal conditions, including as-cast, solution-treated, peak-aged, and over-aged states. Scanning electron microscopy (SEM) and optical microscopy (OM) were employed to examine the crack nucleation and fracture model. The results indicate that the GW94 alloy shows different behaviors of crack initiation and fracture under different thermal conditions. During tensile test at room temperature, the fracture model of the as-cast GW94 alloy is quasi-cleavage, while that of the solution-treated alloy is transgranular cleavage. It is a mixed pattern of transgranular and intergranular fracture for both the aged conditions. Large cavities formed at grain boundaries are observed in the peak-aged sample tested at 300 ˚C, corresponding to the intergranular fracture. Localized plastic deformation at grain boundaries is also observed and corresponds to the high elongation at 300 ˚C.

Key words: magnesium alloy; rare earth; Mg-Gd-Y alloys; mechanical properties; fracture behavior; heat treatment

1 Introduction

Due to the strong demand for weight reduction of transportation vehicles for better fuel efficiency, magnesium alloys recently receive wide research interest for applications to various structural components of automobiles and aircrafts[1−2]. The addition of rare-earth (RE) elements such as Gd, Y, Nd and Dy has been known to improve strength and creep properties[3−8]. It was reported that Mg-Gd-Y system alloys exhibited higher specific strength at both room and elevated temperatures and better creep resistance than conventional Al and Mg alloys[9−10]. Precipitation strengthening is reported to be the main strengthening mechanism in these high strength alloys. The precipitation sequence in Mg-Gd-Y alloys is well documented which starts from β'' formation, followed by the formation of β' and β_1 metastable precipitates before reaching the formation of equilibrium β phase[11−13]. The β' metastable phase in the Mg-Gd-Y alloys has a C base-centered orthorhombic (cbco) structure with a cell size of a=0.64 nm, b=2.22 nm and c=0.52 nm. The β' prismatic plates have been claimed to be responsible for the peak mechanical and creep properties in Mg-Gd-Y alloys at elevated temperatures [9, 14].

In the previous study[14], the microstructure and strengthening mechanisms of a cast Mg-8.57Gd-3.72Y-0.54Zr (mass fraction, %) have been investigated by a combination of thermodynamic calculations and experimental approaches. Besides, the fracture behavior is also important in understanding the relationship between microstructure and mechanical properties, as it determines the fracture strength and elongation. However, the facture behavior of Mg-Gd-Y based alloy is seldom mentioned.

Therefore, in the present work, the fracture behavior evolution of the high strength Mg-Gd-Y-Zr alloy with and without heat treatment is studied. The relationship between mechanical properties and fracture model is also discussed.

2 Experimental

The alloy was prepared from high purity Mg (>99.95%), Gd (>99%), Y (>99%), and a Mg-30Zr (mass

Foundation item: Project(2007CB613704) supported by the National Basic Research Program of China
Corresponding author: HAN En-hou; Tel: +86-24-23926646; Fax: +86-24-2384149; E-mail: ehhan@imr.ac.cn; rongshichen@yahoo.com
DOI: 10.1016/S1003-6326(09)60281-8

fraction, %) master alloy by melting in an electric resistance furnace at about 780 ˚C under the protection of an anti-oxidizing flux. The melt was poured into a mild steel mould preheated to 200−300 ˚C. The actual chemical composition of the alloy was Mg-8.57Gd-3.72Y-0.54Zr (mass fraction, %) (GW94) or Mg-1.48Gd-1.13Y-0.16Zr (molar fraction, %) determined by inductively coupled plasma atomic emission spectroscopy (ICP).

The specimens cut from the cast ingot were solution treated at 525 ˚C for 6 h, quenched into hot water at about 70 ˚C, and then aged at 225 ˚C and 190 ˚C for various periods of time. The Vickers hardness testing was performed using a load of 4.9 N and a holding time of 15 s. Not less than ten measurements were taken in each alloy. The samples for tensile tests had a gauge length of 5 mm, width of 3 mm and thickness of 2 mm. The tensile tests were performed at an initial stain rate of 1.0×10^{-3} s^{-1} and at temperatures between room temperature and 300 ˚C. For tests at elevated temperatures, the specimens were heated up to the selected temperature within 10 min and were soaked for 5 min before testing. The temperature was controlled within ±2 ˚C. Three specimens were used for each test condition to ensure the reproducibility of data.

The fractured specimens were sectioned longitudinally and examined for crack nucleation sites using optical microscopy (OM) and scanning electron microscopy (SEM). The fracture surfaces of the failed tensile specimens were examined using scanning electron microscopy.

3 Results and discussion

3.1 Microstructure of as-cast GW94 alloy

The microstructural evolution of the GW94 alloy in difference thermal conditions has been investigated in our previous studies[14]. It is shown that both $Mg_{24}(Gd,Y)_5$ and cuboid-shaped $Mg_5(Gd, Y)$ phases exist in the as-cast sample, as shown in Fig.1. The former is dissolved during solution treatment, while the latter persists and coarsens. Subsequent artificial ageing results in the precipitation of metastable β' precipitates within the α-Mg matrix and along grain boundaries.

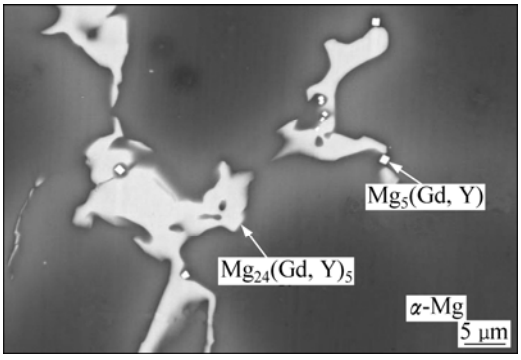

Fig.1 SEM micrograph of as-cast GW94 alloy

3.2 Age hardening behavior

Fig.2 shows the effect of ageing time on the hardness of GW94 alloy during isothermal ageing at 190 and 225 ˚C, respectively. Prior to ageing, the initial hardness of the solution-treated alloy is HV 82. The alloy exhibits ageing hardening behavior both isothermally aged at 190 and 225 ˚C. During isothermal ageing at 190 ˚C, the specimen exhibits higher peak hardness but much slow increase in hardness and longer time to peak (about 130 h), which cannot be acceptable for the industry application. On the other hand, the alloy aged at 225 ˚C takes only 24 h to reach the peak hardness (HV 129). Moreover, the alloy aged at 190 ˚C shows a wide peak hardness plateau from 130 to 338 h with a Vickers hardness of about HV 134 followed by a rapid decline.

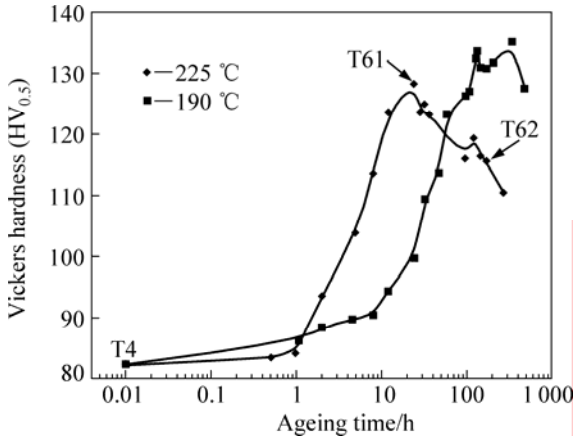

Fig.2 Age hardening curves of GW94 alloy at 190 and 225 ˚C

From Fig.2, we can conclude that when the alloy is aged at 225 ℃ for less than 1 h, the hardness increase is due to the precipitation of β'' phase as commonly observed in Mg-RE (RE: Gd, Y, Nd, Dy, Th) systems[15]. When the alloy is aged for more than 1 h, the formation of β' phase causes hardness to increase rapidly, and the peak hardness is achieved at ageing 24 h. Continuing ageing leads to the coarsening of β' phase[14] and the formation of stable β phase[13], which causes the hardness to decrease quickly. Ageing times of 24 h and 168 h are selected, which correspond peak (T61) and over-aged (T62) conditions, respectively.

3.3 Tensile mechanical properties

The mechanical properties including ultimate tensile strength (UTS), yield strength (YS) and elongation in as-cast (F), solution-treated (T4), peak-aged (T61) and over-aged (T62) conditions are shown in Fig.3. Compared with the as-cast sample, solution treatment results in a great enhancement in elongation accompanied by a relatively small increase in UTS.

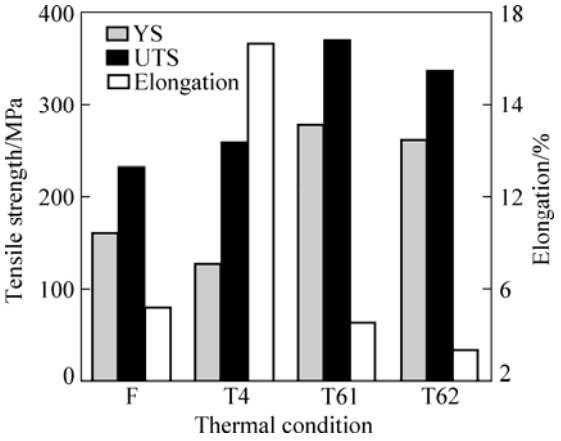

Fig.3 Tensile properties of GW94 alloy in different thermal conditions at room temperature (F: as-cast; T4: 525 ˚C, 6 h (solution-treated); T61: (525 ˚C, 6 h)+(225 ˚C, 24 h) (peak-aged); T62: (525 ˚C, 6 h)+(225 ˚C, 168 h) (over-aged))

GW94 alloy shows the highest tensile strength after isothermal peak-ageing at 225 ˚C with the UTS and YS of 370 MPa and 277 MPa at room temperature, respectively. This strengthening effect is believed to be due to β' precipitation as demonstrated in our previous work [14].

3.4 Fracture behavior at room temperature

The secondary electron (SE) SEM micrographs of the fracture surfaces of the tensile specimens of GW94 alloy under various conditions are shown in Fig.4. In as-cast alloy, the fracture surfaces are composed of cleavage planes and fractured eutectics (Fig.4(a)), which is in accordance with its limited elongation of 5.2%. The fracture model of as-cast GW94 alloy is quasi-cleavage. When the alloy is subjected to solution treatment, the fracture surfaces are mainly composed of ductile transgranular cleavage planes of coarse dimples (river pattern) and tear ridges (Fig.4(b)), which is in accordance with its high elongation of 16.6%. The fracture mode of solution-treated GW94 alloy is transgranular cleavage. After being peak-aged at 225 ˚C, the grain interior is strengthened by coherent β' phase[14] and the fracture surfaces are characterized by cleavage planes and grain boundaries (Fig.4(c)). It is a mixed pattern of transgranular and intergranular fracture. Under the over-aged condition, the fracture surface is characterized mainly by grain boundaries, as shown in Fig.4(d).

Fig.5 shows the SEM microstructures of ruptured samples perpendicular to the fracture surface which are deformed at room temperature. Secondary cracks near the fracture surface are observed. During deformation, damage is produced by the fragmentation of the $Mg_{24}(Gd,Y)_5$ intermetallic particles in as-cast alloy, as shown in Fig.5(a), with the cracks being preferentially perpendicular to the stress axis. As already mentioned, when the alloy is solution treated at 525 ˚C, the eutectics along grain boundaries disappear and the secondary

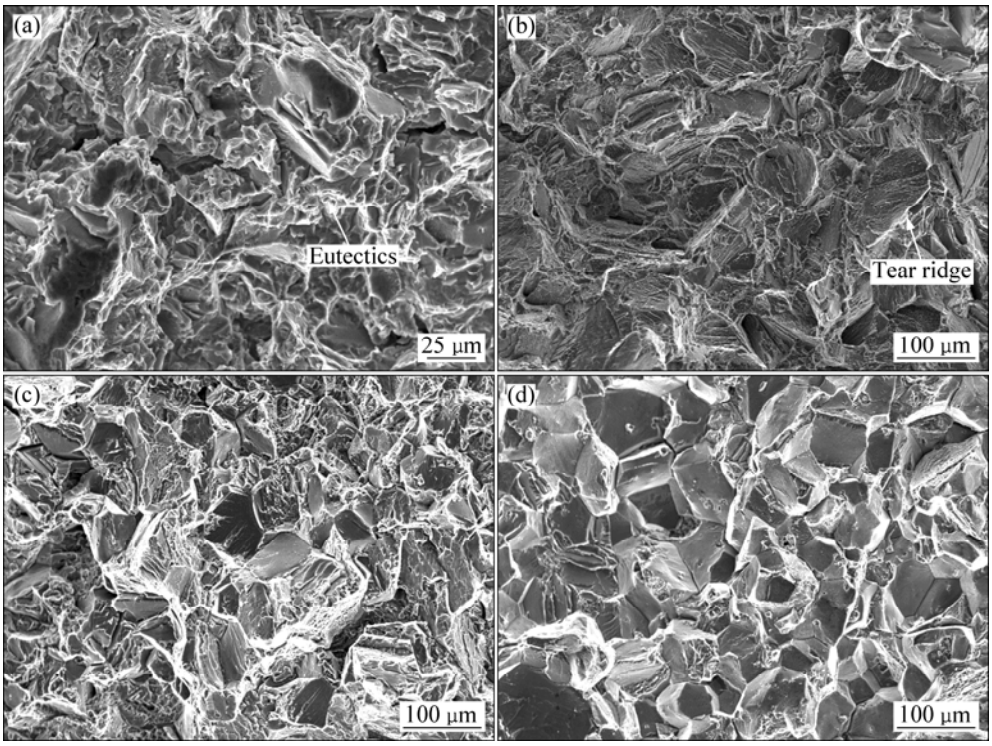

Fig.4 SEM micrographs of fracture surfaces of tensile specimens tested at room temperature: (a) As-cast; (b) Solution-treated; (c) Peak-aged; (d) Over-aged

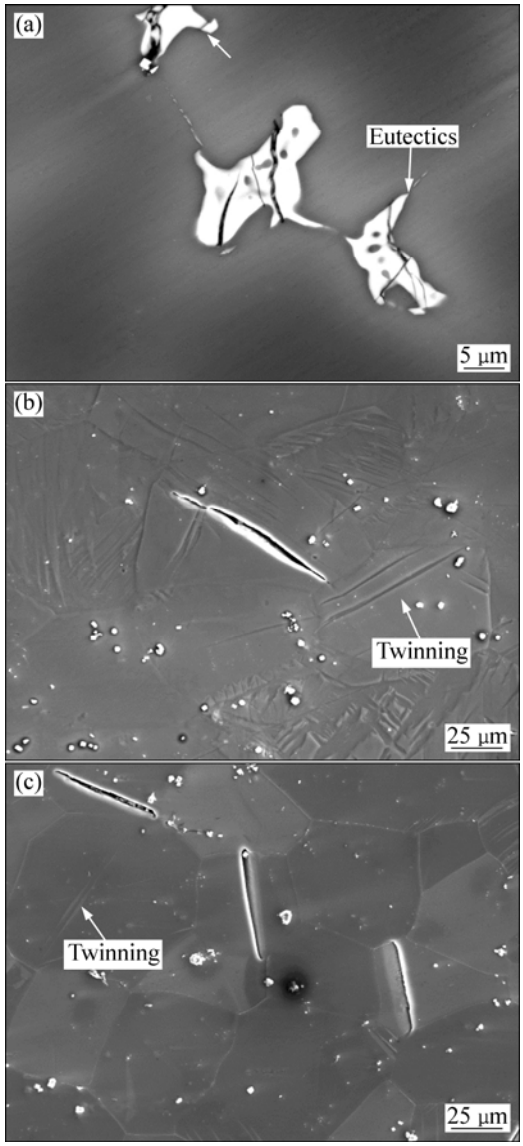

Fig.5 SEM images of longitudinal section of fracture surface of GW94 alloy tested at room temperature in different conditions: (a) As-cast; (b) Solution-treated; (c) Peak-aged

cracks mainly locate inside the grains (Fig.5(b)). The cracks probably initiate at the grain interiors and propagate transgranularly. Followed by ageing at 225 ˚C for 24 h, the secondary cracks are also present at grain interiors (Fig.5(c)). Moreover, deformation twins are observed in the solution-treated and peak-aged samples. Cracks may originate at the twins.

3.5 Fracture behavior at 300 ˚C

It was reported that GW94 alloy has more than 30% elongation at 300 ˚C and the alloy also retained a high strength of more than 300 MPa at 250 ˚C[14]. The fracture behavior of the peak-aged sample tested at 300 ˚C can be seen in Fig.6. It is clear that the fracture surface shows lots of tear ridge near the triple points of grain boundaries (Fig.6(a)), corresponding to localized plastic deformation at grain boundary and high elongation of 31%[14]. Large cavities formed at grain boundaries are observed in Fig. 6(b) and the grains seem to be elongated along the tensile direction. It can be confirmed that the fracture mode changes from transgranular to intergranular fracture with increasing the temperature to 300 ˚C. The coarsening of precipitates and easy gliding on non-basal planes at high temperatures[9] facilitate the deformation, resulting in the intergranular fracture and an increase in elongation. Cracks or voids near the triple points of grain boundaries correspond to the grain boundary sliding for deformation.

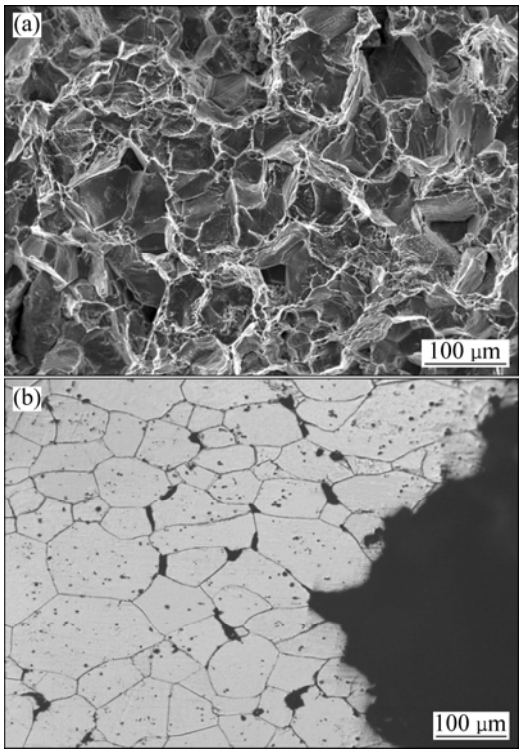

Fig.6 SEM microstructures of fracture surface (a) and optical microstructure of longitudinal section of fracture surface (b) for peak-aged sample tested at 300 ˚C

4 Conclusions

1) The fracture behavior of a permanent mould casting Mg-8.57Gd-3.72Y-0.54Zr (mass fraction, %) (GW94) alloy has been investigated under different thermal conditions, including as-cast, solution-treated, peak-aged and over-aged states. GW94 alloy shows different behaviors of crack initiation and fracture under different thermal conditions.

2) During tensile test at room temperature, cracks form by the break of eutectics along the grain boundaries and propagate transgranularly in the as-cast alloy. After solution-treatment, the cracks probably initiate at the

grain interiors and propagate transgranularly. It is a mixed pattern of transgranular and intergranular fracture for the 225 ˚C peak-aged sample.

3) Localized plastic deformation and large cavities formed at grain boundaries are observed in the peak-aged sample tested at 300 ˚C, corresponding to the intergranular fracture.

References

[1] HONMA T, OHKUBO T, KAMADO S, HONO K. Effect of Zn additions on the age-hardening of Mg-2.0Gd-1.2Y-0.2Zr alloys [J]. Acta Mater, 2007, 55: 4137−4150.

[2] SMOLA B, STULIKOVA I, BUCH F V, MORDIKE B L. Structural aspects of high performance Mg alloys design [J]. Mater Sci Eng A, 2002, 324: 113−117.

[3] HE S M, ZENG X Q, PENG L M, GAO X, NIE J F, DING W J. Microstructure and strengthening mechanism of high strength Mg-10Gd-2Y-0.5Zr alloy [J]. J Alloys Compd, 2007, 427: 316−323.

[4] ANYAWU I A, KAMADO S, KOJIMA Y. Creep properties of Mg-Gd-Y-Zr alloys [J]. Mater Trans, 2001, 42: 1212−1218.

[5] GAO L, CHEN R S, HAN E H. Solid solution strengthening behaviors in binary Mg-Y single phase alloys [J]. J Alloys Compd, 2009, 472: 234−240.

[6] GAO L, CHEN R S, HAN E H. Effects of rare-earth elements Gd and Y on the solid solution strengthening of Mg alloys [J]. J Alloys Compd, 2009, 481: 379−384.

[7] GAO L, CHEN R S, HAN E H. Characterization of dynamic strain ageing in Mg-3.11wt.%Gd alloy [C]//NYBERG E A, AGNEW S R, NEELAMEGGHAM M R, PEKGULERYUZ M O. Magnesium Technology 2009. San Francisco: TMS, 2009: 269−272.

[8] PENG Q M, WU Y M, FANG D Q, MENG J, WANG L M. Microstructures and mechanical properties of Mg-8Gd-0.6Zr-*x*Nd (*x*=0, 1, 2 and 3 mass%) alloys [J]. J Mater Sci, 2007, 42: 3908−3913.

[9] LIU X B, CHEN R S, HAN E H. Effects of ageing treatment on microstructures and properties of Mg-Gd-Y-Zr alloys with and without Zn addition [J]. J Alloys Compd, 2008, 465: 232−238.

[10] LIN L, CHEN L J, LIU Z. Tensile strength improvement of an Mg-12Gd-3Y (wt%) alloy processed by hot extrusion and free forging [J]. J Mater Sci, 2008, 43: 4493−4502.

[11] GAO X, HE S M, ZENG X Q, PENG L M, DING W J, NIE J F. Microstructure evolution in a Mg-15Gd-0.5Zr (wt.%) alloy during isothermal aging at 250 ℃ [J]. Mater Sci Eng A, 2006, 431: 322−327.

[12] YANG Z, LI J P, GUO Y C, LIU T, XIA F, ZENG Z W, LIANG M X. Precipitation process and effect on mechanical properties of Mg-9Gd-3Y-0.6Zn-0.5Zr alloy [J]. Mater Sci Eng A, 2007, 454/455: 274−280.

[13] HE S M, ZENG X Q, PENG L M, GAO X, NIE J F, DING W J. Precipitation in a Mg-10Gd-3Y-0.4Zr (wt.%) alloy during isothermal ageing at 250 ℃ [J]. J Alloys Compd, 2006, 421: 309−313.

[14] GAO L, CHEN R S, HAN E H. Microstructure and strengthening mechanisms of a cast Mg-1.48Gd-1.13Y-0.16Zr (at.%) alloy [J]. J Mater Sci, 2009, 44: 4443−4454.

[15] HONMA T, OHKUBO T, HONO K, KAMADO S. Chemistry of nanoscale precipitates in Mg-2.1Gd-0.6Y-0.2Zr (at.%) alloy investigated by the atom probe technique [J]. Mater Sci Eng A, 2005, 395: 301−306.

(Edited by YANG Bing)